The Central Italy Seismic Sequence between August and December 2016: Analysis of Strong-Motion Observations

by Lucia Luzi, Francesca Pacor, Rodolfo Puglia, Giovanni Lanzano, Chiara Felicetta, Maria D'Amico, Alberto Michelini, Licia Faenza, Valentino Lauciani, Iunio Iervolino, George Baltzopoulos, and Eugenio Chioccarelli

ABSTRACT

Since August 2016, central Italy has been struck by one of the most important seismic sequences ever recorded in the country. In this study, a strong-motion data set, consisting of nearly 10,000 waveforms, has been analyzed to gather insights about the main features of ground motion, in terms of regional variability, shaking intensity, and near-source effects. In particular, the shake maps from the three main events in the sequence have been calculated to evaluate the distribution of shaking at a regional scale, and a residual analysis has been performed, aimed at interpreting the strong-motion parameters as functions of source distance, azimuth, and local site conditions. Particular attention has been dedicated to near-source effects (i.e., hanging wall/footwall, forward-directivity, or fling-step effects). Finally, ground-motion intensities in the near-source area have been discussed with respect to the values used for structural design.

In general, the areas of maximum shaking appear to reflect, primarily, rupture complexity on the finite faults. Large ground-motion variability is observed along the Apennine direction (northwest–southeast) that can be attributed to source-directivity effects, especially evident in the case of small-magnitude aftershocks. Amplifications are observed in correspondence to intramountain basins, fluvial valleys, and the loose deposits along the Adriatic coast. Near-source ground motions exhibit hanging-wall effects, forward-directivity pulses, and permanent displacement.

INTRODUCTION

Since August 2016, an extended region of central Italy has experienced a long-lasting seismic sequence (still active at the time of submission of this work). Until December 2016, three main events with magnitude larger than 5.5 (Fig. 1) struck an area approximately more than 50 km long and 30 km wide. The initiating event was the Amatrice earthquake (M_w 6.0), which occurred on 24 August 2016 at 1:36:32 UTC and strongly damaged the villages of Amatrice and Accumoli. Despite the fact that the population exposed to VIII+ Mercalli–Cancani–Sieberg (MCS) intensity was relatively small (7500 to 10,000 inhabitants), the earthquake caused about 300 fatalities due to the collapse of several buildings in the towns and villages closest to the epicenter. A second event (M_w 5.9), occurred farther north, on 26 October2016 at 19:18:06 UTC, near the village of Ussita (Fig. 1), and resulted in additional damage to the buildings and main infrastructures previously hit by the 24 August event. The third and largest event (M_w 6.5) occurred on 30 October 2016 at 06:40:18 UTC; the epicenter was located close to Norcia (Fig. 1). It caused the total collapse of several structures damaged by the previous events and the complete destruction of the village of Amatrice. Fortunately, there were no fatalities caused by the October events; most of the population had been evacuated already. These seismic events triggered extended secondary effects such as ground failures (widespread surface faulting, ground cracks, and landslides) and deep-seated landslides as described by Huang *et al.* (2017) and Pucci *et al.* (2017).

The area affected by the sequence is located in the central Apennine belt in Italy, a region characterized by crustal extension, where north-northwest–south-southeast and northwest–southeast (NW–SE)-striking normal and normal-oblique faults, active since the early Quaternary, are superimposed to a pre-existing strike-slip and fold-and-thrust belt structure (Calamita and Pizzi, 1994; Lavecchia *et al.*, 1994, 2002; Cello *et al.*, 1997; Vezzani *et al.*, 2010). The fault segments generally dip southwestward, extending 20–25 km along strike and 10–15 km along dip (Boncio *et al.*, 2004). Their typical en echelon pattern locally originates intramountain basins, such as the Norcia plain (Boncio and Lavecchia, 2000; Galadini and Galli, 2000).

Moderate and strong seismic events struck this area in the past decades (the 1984 M_w 5.6 Gubbio, 1997 M_w 6.0

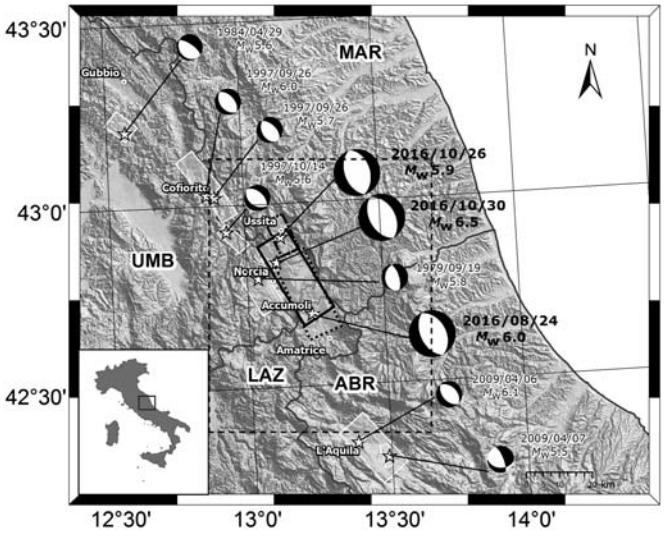

▲ **Figure 1.** Geographic overview of the study area (administrative regions: LAZ, Lazio; ABR, Abruzzo; MAR, Marche; UMB, Umbria). White rectangles are the surface fault projections of the main seismic events that have occurred since 1979 (from Engineering Strong Motion [ESM]); black rectangles are the fault projections of the events relative to the 2016 seismic sequence from Chiaraluce *et al.* (2017): the continuous line is relative to the M_w 6.5 Norcia event, whereas the dashed line is the M_w 6.0 Amatrice event. The large rectangle (dashed black line) sketches the area detailed in Figure 2

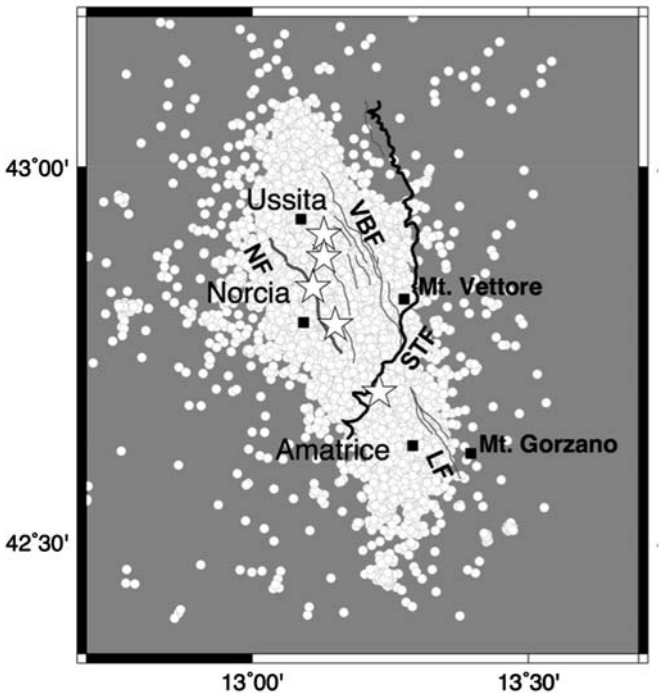

▲ **Figure 2.** Aftershocks from 24 August to 1 December 2016 (white circles, from Chiaraluce *et al.*, 2017); location of the five events with **M** >5 (white stars); main tectonic features of the area (black and gray lines). VBF, Mt. Vettore–Mt. Bove fault system; LF, Laga fault system; NF, Norcia fault; STF: Mts. Sibillini thrust.

Colfiorito, 1979 M_w 5.9 Norcia, and 2009 M_w 6.1 L'Aquila events; see Fig. 1). All these earthquakes featured focal mechanisms consistent within the regional northeast–southwest (NE–SW) tensional stress field.

The three mainshocks of the central Italy sequence occurred along a fault alignment that extends from Mt. Vettore to Mt. Bove to Mt. Gorzano (VBF and LF, respectively, in Fig. 2). It lies to the east of the alignment that develops from Gubbio to Colfiorito, and extends as far as the area struck by the 2009 L'Aquila sequence to the south (Fig. 1).

The causative fault mechanism of the three mainshocks herein considered, obtained from Time Domain Moment Tensor technique (Dreger and Helmberger, 1993) and implemented at Istituto Nazionale di Geofisica e Vulcanologia (INGV) National Earthquake Centre (Scognamiglio *et al.*, 2010), features pure normal faulting, in agreement with the prevailing extensional regime of the central Apennines and with the mechanisms of the Colfiorito and L'Aquila earthquakes (Scognamiglio *et al.*, 2016). The characteristics of these events are reported in Table 1.

The aim of this work is to provide (1) a description of the ground motion associated with the sequence between August and December 2016 through the comparison with ground-motion prediction equations (GMPEs), analyzing the nearly 10,000 waveforms recorded for the mainshocks and the 48 aftershocks with moment magnitude larger than or equal to 4; (2) an interpretation of the strong-motion parameters as a function of the distance to the source, azimuth, and local site

Table 1
Characteristics of the Three Main Events

Date (yyyy/mm/dd hh:mm:ss)	M_w*	Depth (km)†	Latitude†	Longitude†	Strike*	Dip*	Rake*	Width (km)	Length (km)
2016/08/24 01:36:32	6.0	7.93	42.70	13.25	156	50	−85	16‡	26‡
2016/10/26 19:18:05	5.9	7.5	42.91	13.13	159	47	−93	10§	18§
2016/10/30 06:40:17	6.5	9.4	42.84	13.11	151	47	−89	14§	26§

*Obtained from Time Domain Moment Tensor (TDMT, see Data and Resources).
†Obtained from Centro Nazionale Terremoti (CNT, see Data and Resources).
‡From Tinti *et al.* (2016).
§From Chiaraluce *et al.* (2017).

conditions, with particular emphasis on near-source effects; and (3) a discussion on the shaking intensity with respect to the structural design values in the area.

As expected, ground-motion intensity in the near fault is significantly influenced by the rupture mechanism, the direction of rupture propagation relative to the site, and possible permanent ground displacements resulting from the fault slip. In this work the term directivity is often used. Typically, seismological literature will reserve the term directivity for phenomena linked to rupture propagation. One consequence of such phenomena is the azimuthal dependence of amplification/deamplification of the ground-shaking intensity, with a maximum when the site is located in the forward direction with respect to the rupture propagation. It has also been observed that sites aligned with both the direction of the horizontal *S*-wave radiation pattern lobe and the direction of rupture propagation may exhibit velocity traces of an impulsive nature and consequent narrowband spectral amplification (e.g., Somerville *et al.*, 1997; Spudich *et al.*, 2014), often referred to as pulse-like ground motion. Engineering-oriented publications have been known to use the term directivity to cover all of the above cases, especially pulse-like effects. In the present work, the term directivity will be used according to the seismological approach, whereas the occurrence of impulsive waveforms attributable to constructive interference of *S* waves will be referred to as pulse-like directivity effects. It is also relevant to mention that recordings of near-fault ground motions may contain permanent ground displacements due to the static deformation field of the earthquake, an effect typically termed fling step. Fling step, which is associated with a large amplitude, a half-cycle velocity pulse, and a monotonic step in the displacement trace, is also examined in the present article.

STRONG-MOTION DATA SET

As mentioned, nearly 10,000 waveforms were recorded since 24 August to December 2016 in the area struck by the sequence. They are of major relevance not only for a complex regional context such as Italy, but also at the worldwide scale, because they increase the set of normal fault and near-source recordings that are usually poorly represented in global strong-motion databases (e.g., REference database for Seismic grOund-motion pRediCtion in Europe [RESORCE], Akkar *et al.*, 2013; Next Generation Attenuation [NGA]-West2, Darragh *et al.*, 2014).

The record set has been made available by the Italian Accelerometric Network Rete Accelerometrica Nazionale (RAN; Presidency of the Council of Ministers, Civil Protection Department, 1972), managed by the Department of Civil Protection (DPC), and the Italian seismic network, managed by INGV (Rete Sismica Nazionale [RSN]; INGV Seismological Data Centre, 1997). After the Amatrice event, INGV and DPC installed about 35 temporary stations to monitor the earthquake sequence at higher resolution to obtain more accurate values of the source parameters and of the ground shaking in the near-source region.

The recording sites are classified according to Eurocode 8 (2003; hereafter, EC8), based on the shear-wave velocity averaged over the top 30 m of the soil profile, V_{S30} (in which EC8 class A > 800 m/s, B = 360–800 m/s, C = 180–360 m/s, and D < 180 m/s), available for 30 sites out of a total of 230. In cases where the geological/geophysical information is not available, the class has been inferred from the surface geology (Di Capua *et al.*, 2011; Felicetta *et al.*, 2017). The majority of stations belong to class A or B, whereas a few stations are classified as C.

The accelerometric records are manually processed using the procedure described by Paolucci *et al.* (2011), which prescribes the application of a second-order acausal time-domain Butterworth filter to the zero-padded acceleration time series and zero-pad removal to make acceleration and displacement consistent after double integration. The typical band-pass frequency range is between 0.08 and 40 Hz because the entire set is composed of digital records. The spectral ordinates used for the analysis are selected only within the usable frequency band, defined by the band-pass frequencies. All records, as well as peak ground acceleration (PGA), peak ground velocity (PGV), and spectral acceleration (SA), 5% damped, calculated at T = 0.3, 1.0, and 3.0 s, are public and available at the Engineering Strong-Motion (ESM) database (see Data and Resources). SA will be used in the following sections as a proxy for pseudo-spectral acceleration (PSA) for the shake maps calculation.

The data set of the largest shock (M_w 6.5) consists of 235 records (217 are good quality), with epicentral distances ranging from 5 km to about 410 km and Joyner–Boore distances (R_{JB}) from 0 to 402 km (closest distance to the fault's surface projection; Joyner and Boore, 1981; Kaklamanos *et al.*, 2011); 26 stations have epicentral distances less than 30 km, and 4 stations have R_{JB} < 1 km.

In general, PGAs recorded at epicentral distances shorter than 15 km are greater than 350 cm/s^2, and vertical PGAs are of the same order as that of horizontal components within 10 km from the epicenter. PGVs recorded at epicentral distances less than 15 km are in general greater than 10 cm/s.

The largest recorded absolute PGAs are: 850 cm/s^2 (east–west [E-W] component of the station AMT, on 24 August), 869 and 782 cm/s^2 (vertical or Z component of the stations T1213 and CLO, respectively, on 30 October), and 638 cm/s^2 (E-W component of station CMI, on 26 October). The largest absolute PGVs were recorded during the 30 October event (M_w 6.5): 83 cm/s (E-W component of the temporary station T1201), 54 cm/s (E-W component of the temporary station T1214), 69 cm/s (Z component of the temporary station CLO), 61 cm/s (E-W component of temporary station T1213), and 48 cm/s (E-W component of the stations NRC and NOR).

SHAKE MAPS

The distribution of the ground shaking has been determined using the ShakeMap software (Wald *et al.*, 1999). Shake maps are routinely calculated by INGV (Michelini *et al.*, 2008; see Data and Resources) using accelerometric and nonsaturated broadband recordings. Maps that are published within a few

minutes from earthquake occurrence are based on peak values after automatic data processing. For $\mathbf{M} \geq 4.0$ earthquakes, revised shake maps are determined using the quality-controlled ground-motion values of the ESM database (see Data and Resources). The finite fault is constructed around the epicenter using the available moment tensor solutions, and the empirical relations by Wells and Coppersmith (1994) for $\mathbf{M} \geq 5.5$ earthquakes and the GMPEs by Akkar and Bommer (2010) are used to predict ground motion when data are unavailable. The site correction is implemented using the 1:100,000 scale Italian geological map, compiled and published by the Servizio Geologico Nazionale (see Data and Resources), by sorting the geological units into five different soil classes according to EC8 (Eurocode 8, 2003). The adopted map has been sampled at a space interval of 1 min for the ShakeMap program. For the amplification factors, the Borcherdt relation is adopted (Borcherdt, 1994), based on V_{S30} values. Overall, the ShakeMap procedure seeks to produce reasonable estimates at grid points located far from available data, while preserving the detailed shaking information available for regions in the vicinity of recording stations (Wald *et al.*, 1999). This implies that, where dense networks are available, the resulting maps depend strongly on the recorded data, while other parameters/information used to generate the maps (e.g., GMPEs or finite-fault extents) become secondary. For this reason, it may occur that the largest ground-motion amplitudes do not occur in correspondence to the projection of the adopted fault, as explained above.

The shake maps of the three main events of the sequence mainshocks are shown in Figure 3, which is organized as follows: the figure columns refer to the three mainshocks whereas the rows refer to the ground-motion shake maps in terms of MCS intensity (converted from ground-motion parameters adopting the relation of Faenza and Michelini, 2010), PGA, PGV, and PSA at $T = 3.0$ s.

The ground-shaking patterns shown in Figure 3 indicate that the largest PGAs are distributed along the Apennine direction (NW–SE). In particular, in the case of the M_w 5.9 Ussita earthquake, large PGAs are observed to the north, likely resulting from source rupture directivity effects. The presence of intramountain basins (e.g., Castelluccio plain), alluvial valleys (e.g., Valle Umbra), and geologic settings such as the Plio–Pleistocene sediments along the Adriatic coast to the NE results in observed local amplifications of PGV and long-period acceleration response (PSA $T = 3.0$ s). A general common feature shared by the three main earthquakes is the rapid decay of PGAs and PGVs toward west-southwest.

RESIDUAL ANALYSIS

The residual analysis of strong-motion data (Rodriguez-Marek *et al.*, 2011; Luzi *et al.*, 2014) is essential to identify the role of source and site in the variability of ground motion, and to evidence path effects or features that are not accounted for by GMPEs. Residuals (R_{es}) are computed as the difference between the logarithm of observations and predictions, in which the GMPE by Bindi *et al.* (2011) has been assumed as reference for PGA and SA. The contribution of the sources and the random variability (Al Atik *et al.*, 2010) is evaluated through the breakdown of the residuals according to:

$$R_{es} = \delta B_e + \delta W_{es}, \tag{1}$$

in which the subscripts e and s denote events and stations, respectively.

δB_e is the between-event residuals (event term), which represent the average deviation of one particular earthquake with respect to the median ground-motion prediction, calculated as the mean of residuals per event; δW_{es} represents the within-event residual.

The standard deviation of the between-event residual is in the 0.38–0.54 range in natural log scale. These values are comparable to the Italian and European GMPEs (Bindi *et al.*, 2011, 2014) and are slightly lower than the global model by Cauzzi *et al.* (2015).

We make use of the within-event residuals to calculate the site term for each station s:

$$\delta S2S_s = \frac{1}{NE_s} \sum_{e=1}^{NE_s} \delta W_{es}, \tag{2}$$

in which NE_s is the number of earthquakes recorded by the station s (minimum number considered is 5).

The within-event residual can be decomposed as:

$$\delta W_{es} = \delta S2S_s + \delta WS_{es}, \tag{3}$$

in which δWS_{es} is the site- and event-corrected residuals and represents the component of the residual after the removal of the repeatable effects of sources and sites.

Figure 4 shows the plot of the within-event (δW_{es}) and the site- and event-corrected residuals (δWS_{es}) in function of the source-to-site distance and station azimuth, respectively, for PGA, PGV, and SA at $T = 3$ s, for the 48 earthquakes considered in this analysis.

As we examine a single-source zone, stations have nearly constant source-to-site distances; therefore, the within-event residuals (δW_{es}) are considered to explain attenuation effects, because the site term may also include the attenuation term. On the other hand, we refer to the site- and event-corrected residuals (δWS_{es}) to explain the effects on ground motion due to the rupture process (e.g., hanging wall [HW]/footwall [FW], directivity, or near-source effects).

The plot of δW_{es} versus the source-to-site distance indicates that the GMPE used as reference has a negative trend at distances larger than 60 km, which is larger for PGA and reduces at longer periods that could be attributed to a stronger attenuation with distance, when compared with the predictions. A positive trend is instead observed at short distances, indicating a lack of fit of the GMPE with the near-source records.

The δWS_{es} residuals plotted versus station azimuth (Fig. 5), calculated as the angle between the north and the line connecting the epicenter and the station, indicate that the largest ground-motion variability occurs in correspondence to the

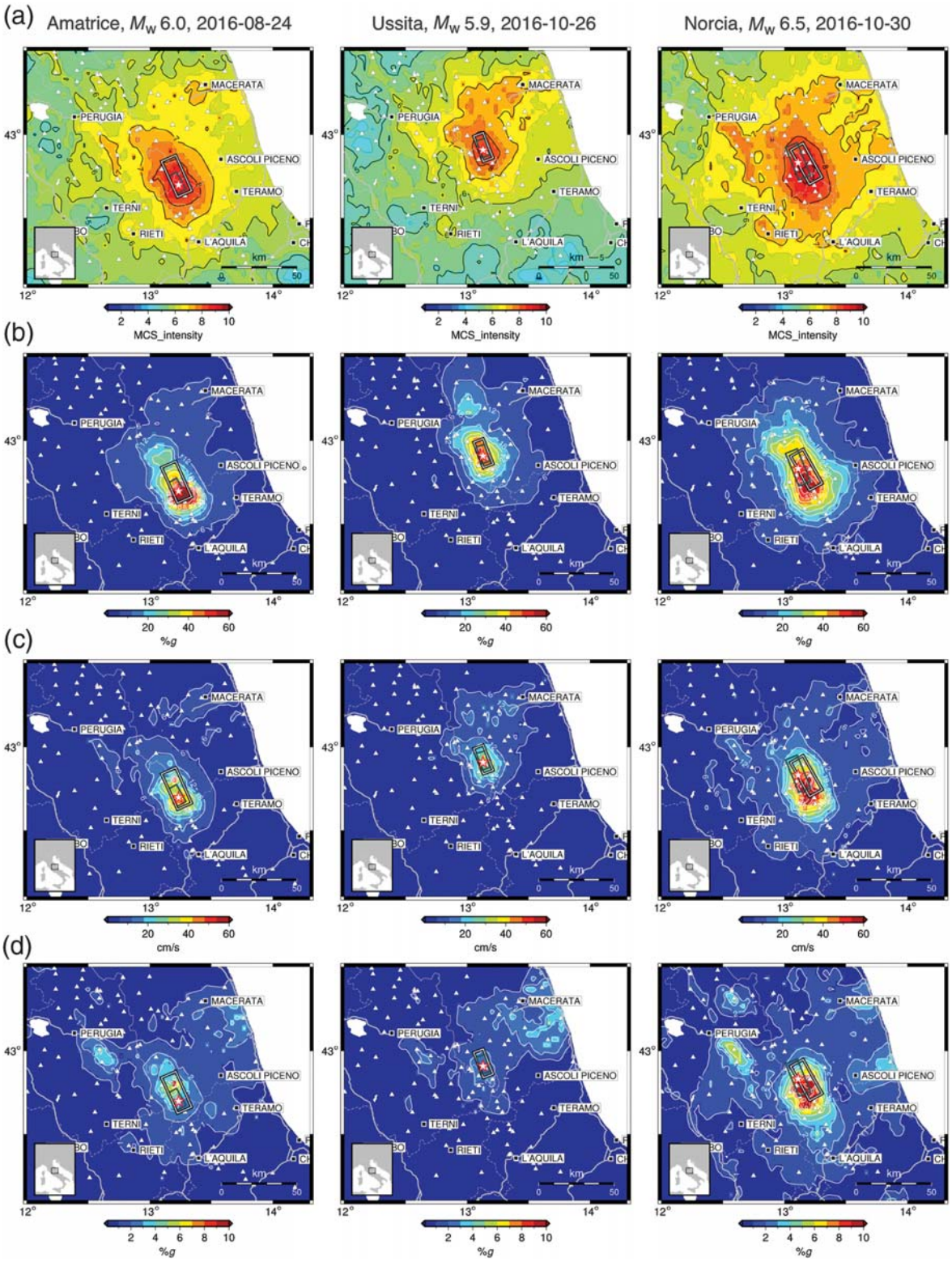

▲ **Figure 3.** Shake maps of the three main events of the central Italy seismic sequence. (Left) Amatrice, 24 August; (center) Ussita, 26 October; (right) Norcia, 30 October. (a) Mercalli–Cancani–Sieberg (MCS) intensity, (b) peak ground acceleration (PGA, %*g*), (c) peak ground velocity (PGV, cm/s), and (d) pseudospectral acceleration (PSA) ($T = 3.0$ s) (%*g*). Stations used to generate the shake map are shown as open triangles, major cities as black squares, region boundaries as dashed gray lines, and main roads as gray thick lines. The epicenters are shown as red-contoured open stars. The surface projection of each fault, used to generate the shake maps, is shown as thick black lines, whereas the black-bordered, white, thick lines show the fault projections of the 2016 seismic sequence main events according to Tinti *et al.* (2016) and Chiaraluce *et al.* (2017).

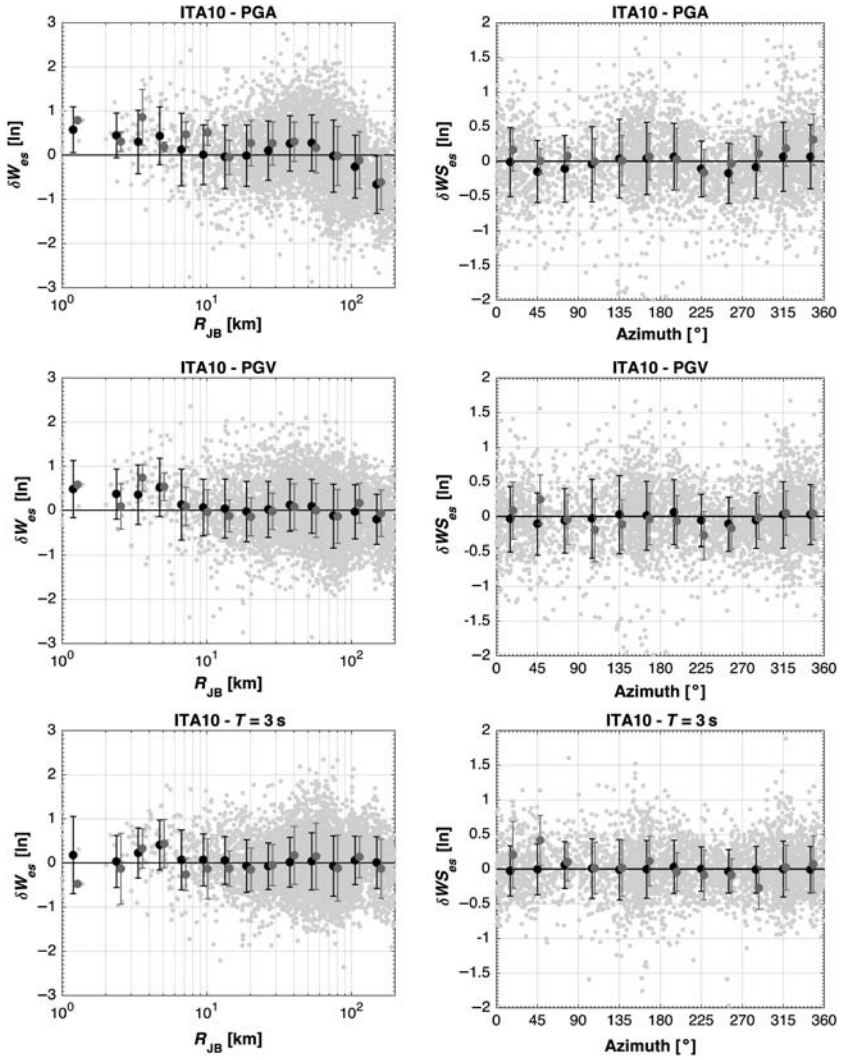

▲ **Figure 4.** Results of the residual analysis. (Left) Within-event residuals (δW_{es}) versus Joyner–Boore distances (R_{JB}, km); (right) event- and site-corrected residuals (δWS_{es}) versus station azimuth. From top to bottom: PGA, PGV, and spectral acceleration (SA) at $T = 3$ s. Black dots and black bars indicate the median and the standard deviation of aftershocks binned by R_{JB} or azimuth; gray dots and gray bars indicate the median and the standard deviation of the three main events for the same R_{JB} or azimuth bins; stations having R_{JB} equal to 0 km have been set to 1 km due to the logarithmic scale representation.

fault strike (e.g., N135–N180 and N315–N360) and affects low to intermediate periods (e.g., PGA and PGV). This variability, also observed in the shake maps, may be attributed to source directivity.

The δWS_{es} of the three main events versus the station azimuth are plotted and mapped in Figure 5a–c, in which PGA is selected as proxy of short periods, which are mainly affected by source directivity. The M_w 6.0 Amatrice event shows a weak directivity in the azimuth range N300–N30, whereas stronger directivity in the azimuth range N315–N10 is observed for the M_w 5.9 Ussita event. The strongest event of the sequence shows a weak directivity to the opposite direction (south–south-southeast). The residual analysis also evidences strong directivity effects for the aftershocks of this sequence that deserve in-depth analysis. In particular, a striking example is the M_w 4.2 event occurred on 3 September 2016 at 01:34:12 UTC (Fig. 5d) that exhibits a strong directivity toward the north (N)–NW.

The δWS_{es} are also plotted, in Figure 6, against the R_x distance, defined by Kaklamanos *et al.* (2011) in NGA-West, to explore HW effects. R_x is computed from the surface projection of the top edge of the rupture plane, perpendicular to the strike: positive values of R_x correspond to the fault HW, whereas negative values correspond to the FW.

Usually HW effects are accounted for in functional forms by introducing the R_{JB} as predictor variable. Using R_{JB}, some of the HW effects are accounted for, as sites directly above the HW are assigned zero distances (Abrahamson and Somerville, 1996). Large δWS_{es} values at positive R_x show HW effects that are not accounted for in Bindi *et al.* (2011), as shown in Figure 6 for the PGA of the three main events. δWS_{es} are also compared with the prediction by Donahue and Abrahamson (2014), calibrated on simulations of thrust-fault events (for magnitude larger than 6.0): the trend of δWS_{es} with distance is in agreement with the model and the largest residuals are observed at distances comparable to the fault width. A similar trend has been observed by Donahue and Abrahamson (2014) for the L'Aquila event, which is also characterized by normal faulting.

OBSERVED VERSUS SEISMIC DESIGN GROUND MOTIONS

This section provides a discussion on the ground-motion intensities recorded during the sequence and the values used for design, according to the Italian seismic code (CS.LL.PP., 2008; hereafter, NTC08). Because the NTC08 design spectra are *de facto* uniform hazard spectra (UHS) from probabilistic seismic-hazard analysis (PSHA; Stucchi *et al.*, 2011), this investigation can also be considered as a comparison between the ground motions recorded during the sequence and the reference values from PSHA; the conceptual limitations of this kind of comparison that the reader should keep in mind are discussed in Iervolino (2013).

Four events with magnitude larger than 5 are considered: the three main events examined in the previous sections and the 26 October 2016 M_w 5.4 event. The stations with the largest horizontal PGA for each event are selected: AMT for the M_w 6.0, CMI for the M_w 5.4 and 5.9, and T1213 (temporary station) for the M_w 6.5 earthquakes. The observed PSAs, at 5% of critical damping, are compared with the elastic design spec-

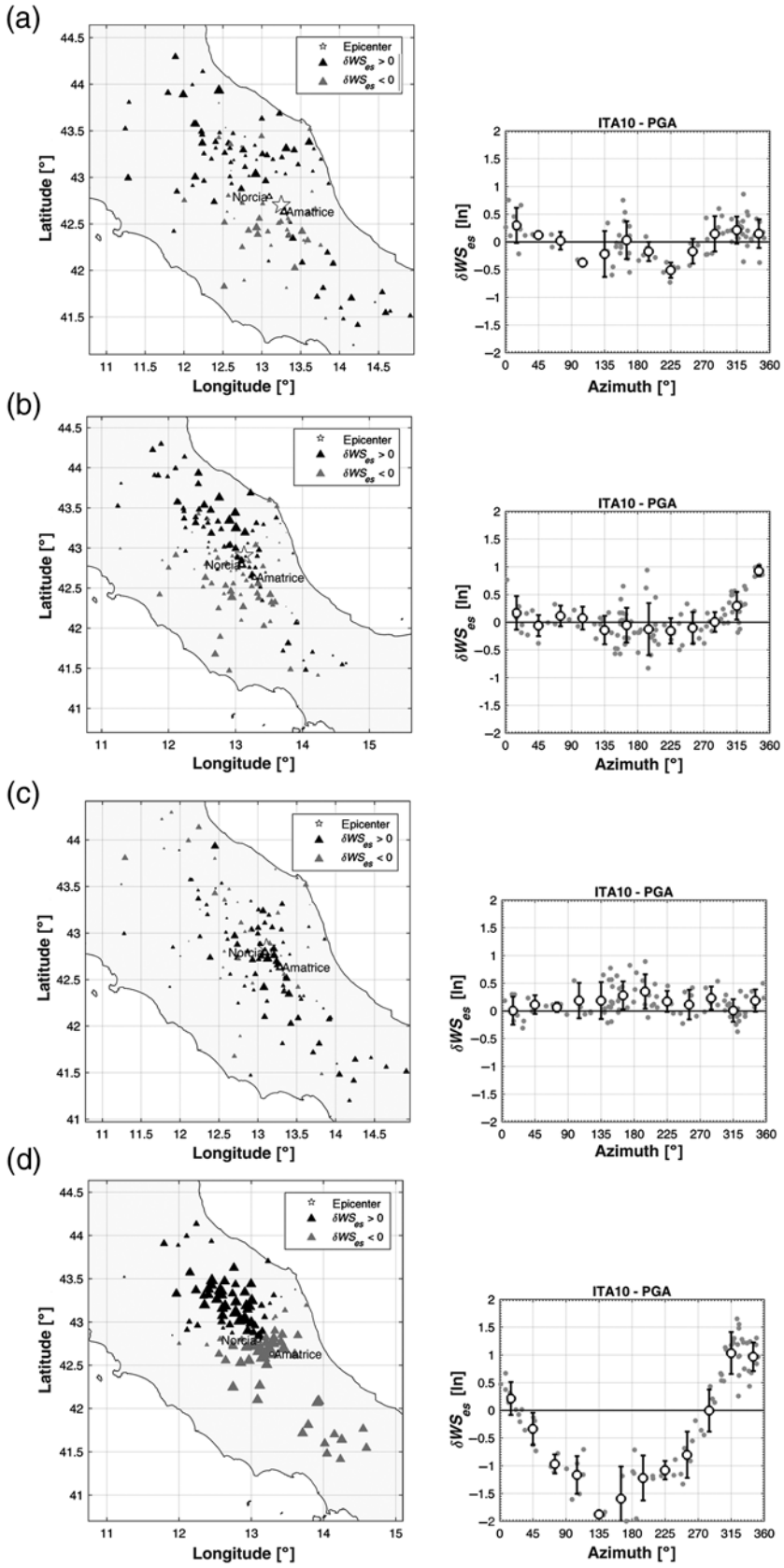

▲ **Figure 5.** Event- and site-corrected residuals δWS_{es} (the spatial distribution is shown in the left column, whereas the azimuthal distribution, where azimuth is calculated from the north, is shown in the right column): (a) 24 August 2016 M_w 6.0; (b) 26 October 2016 M_w 5.9; (c) 30 October 2016 M_w 6.5; and (d) 3 September 2016 M_w 4.2.

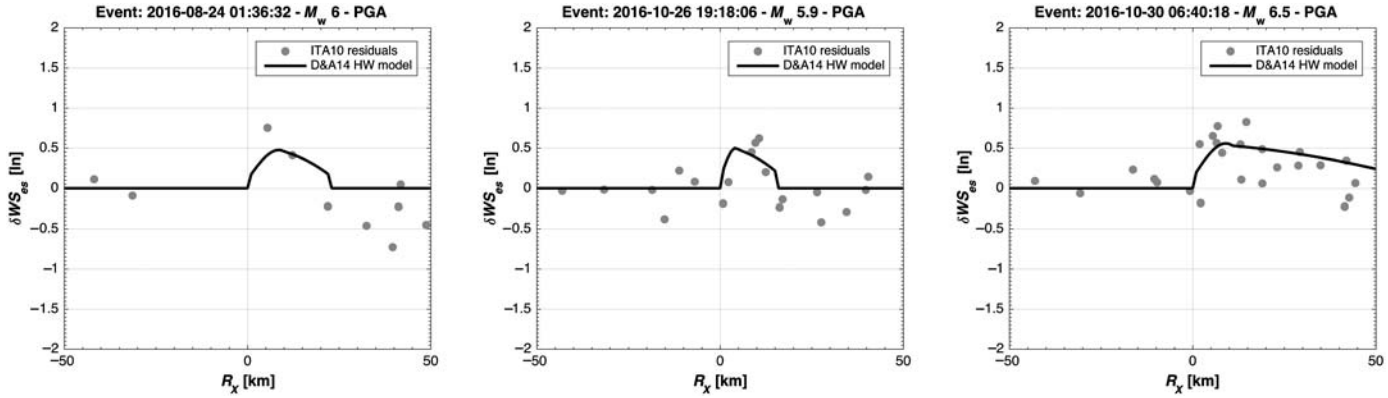

▲ **Figure 6.** PGA δWS_{es} as a function of R_x distance (Kaklamanos *et al.*, 2011). The data are within $R_y < 10$ km (in which R_y is the horizontal distance off the end of the rupture measured parallel to the strike, as in Abrahamson *et al.*, 2014). HW, hanging wall.

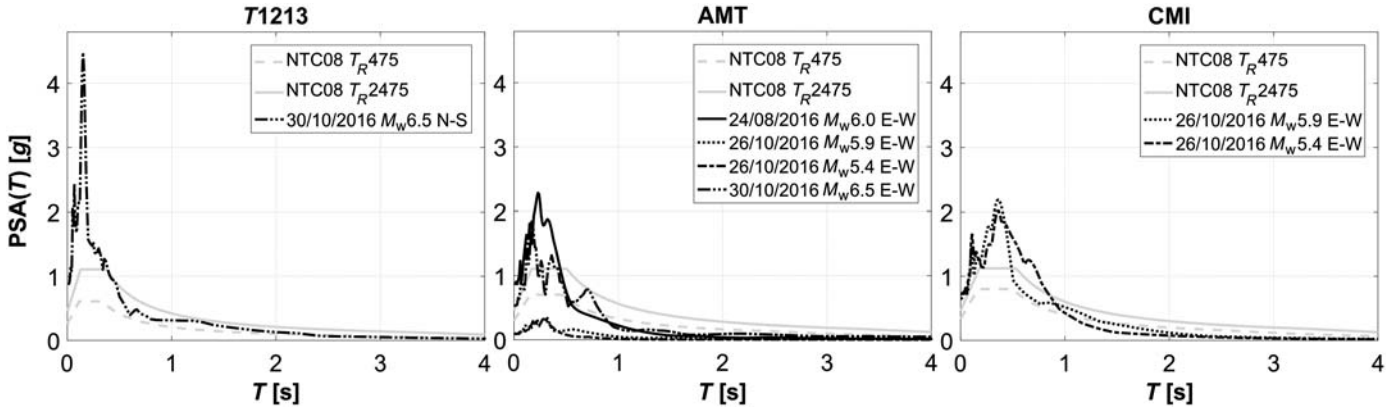

▲ **Figure 7.** Comparisons between NTC08 (CS.LL.PP., 2008) design spectra and elastic spectra from the recording station with the highest PGA in each event.

tra provided by the NTC08 for two different return periods (T_R), for example, 475 and 2475 years. Comparisons are reported in Figure 6; for each station, the spectrum of the horizontal component with the largest peak is reported—that is, E-W components for both AMT and CMI and NS for T1213. The NTC08 spectra are computed for the EC8 soil categories (Eurocode 8, 2003) reported in ESM (see Data and Resources); for example, soil class B for AMT, soil class C for CMI, and soil class A for T1213. Only the AMT station recorded all four considered events whereas ground motions from the M_w 6.0 and 6.5 events are not available for CMI; finally, T1213 provided data only for the M_w 6.5 event.

As shown in Figure 7, in the 0–0.8 s period range (of interest to structural engineering), records exceed the design spectra, when $T_R = 2475$ years is considered. Spectral ordinates rapidly fall as the vibration period increases, which is expected for moderate magnitude events recorded close to the source. In fact, exceedance of design actions is expected to occur for large earthquakes recorded at near-source stations. This is because UHS is likely to be exceeded when the considered site is in the vicinity of the seismic source (for a discussion, see Iervolino, 2013). On the other hand, at larger distances the design spectra are expected to be larger than observations (Iervolino *et al.*, 2016; ReLUIS-INGV Working Group, 2016). This is illustrated via statistics of the spectral exceedances of design values recorded during the M_w 6.5 event (217 stations). For $T_R = 475$ years, it results that 6.9%, 6.9%, and 5.1% of the stations recorded intensity exceeding the corresponding design values for PGA, PSA($T = 0.3$ s), and PSA($T = 1.0$ s), respectively. Considering $T_R = 2475$ years, exceedance statistics become 3.2%, 3.2%, and 2.8%. These results are also shown in Figure 8, in which the 60 stations with epicentral distance shorter than 70 km are shown.

PULSE-LIKE GROUND MOTIONS

Pulse-like near-source ground motions may be the result of rupture forward directivity and the radiation pattern of the seismic source. More specifically, there is a possibility that seismic waves generated at different points along the rupture front will arrive at a properly aligned near-source site simultaneously. This can lead to a constructive wave interference effect, which is manifested in the form of a double-sided velocity pulse that

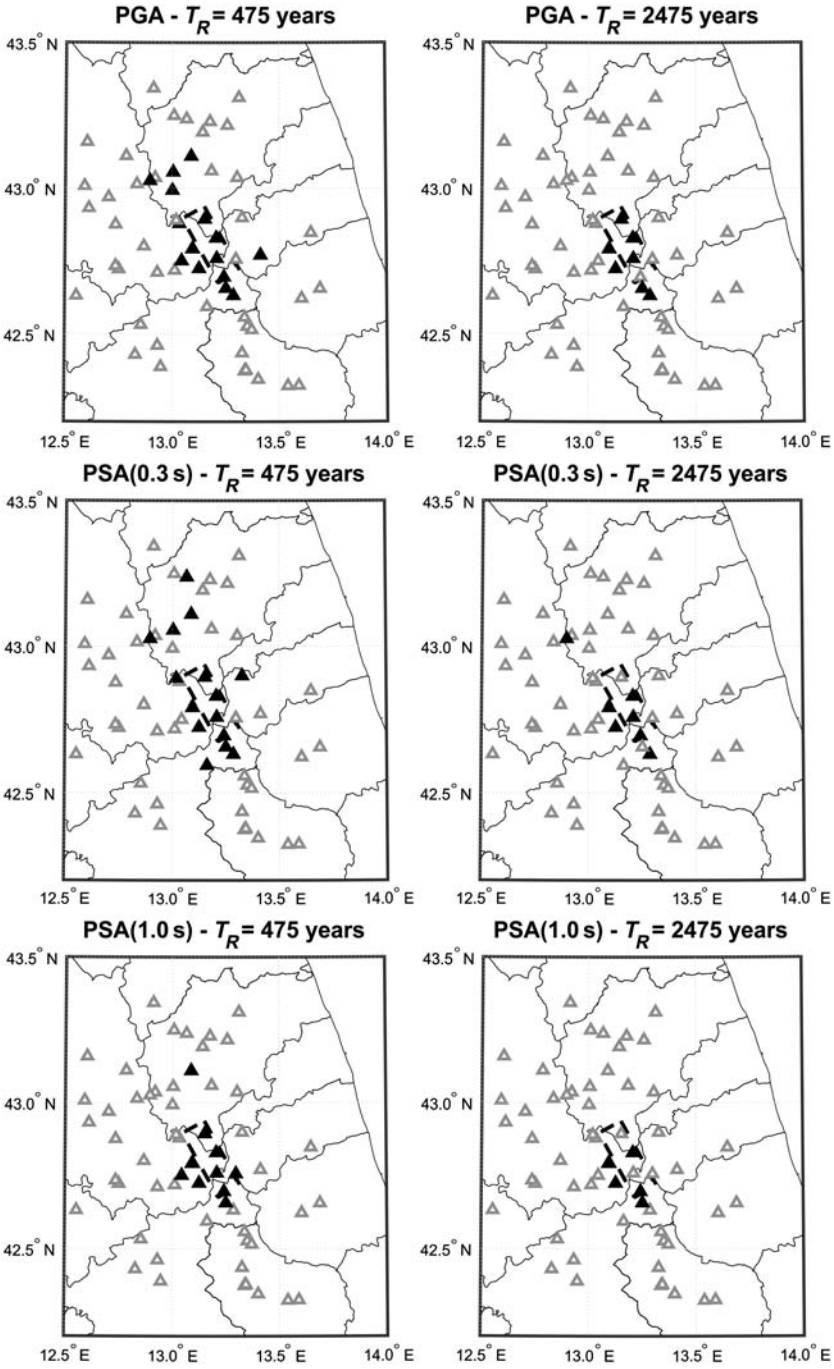

▲ **Figure 8.** The M_w 6.5 Norcia event: map of the differences between observed PGA, PSA(T = 0.3 s) and PSA(T = 1.0 s) and NTC08 design values, for stations within 70 km from the epicenter; black triangles are NTC08 exceedances; gray triangles show stations with spectral amplitudes lower than the code; on the left T_R = 475 years, on the right T_R = 2475 years.

delivers most of the seismic energy early in the record (Somerville *et al.*, 1997).

Besides dynamic effects due to directivity, permanent deformation of the soil (fling step) is another possible near-source effect that can result in impulsive ground-motion attributes. Fling step is the result of either wave propagation generated from a finite dislocation (coseismic slip on the fault) or of the plastic response of near-surface materials (Boore and Bommer, 2005). In the seismic signal, the fling step is identified by a peak in the velocity trace, which can sometimes be regarded as a one-sided pulse (Bolt, 2006), and by a step in the corresponding displacement time series.

Forward-Directivity Pulses

Impulsive ground motions are of particular interest in the context of earthquake engineering, due not only to the amplifying effect on shaking intensity, but also due to their increased (in some cases) damage potential with respect to ordinary, for example, non-pulse-like motions (e.g., Iervolino *et al.*, 2012). Quantitative evidence of such effects can be obtained directly from the velocity traces of recorded motion, using an empirically calibrated algorithm based on the continuous wavelet transform, proposed by Baker (2007). This approach is implemented for the horizontal strong-motion waveforms recorded during the three main events and the 26 October 2016 M_w 5.4 shock. It should be noted that this pulse identification method is phenomenological and does not directly relate positive detections with the physical rupture process itself; as such, relating pulse-like triggers to directivity entails a degree of analyst judgment. Eighteen ground motions are identified as exhibiting possibly directivity-related impulsive characteristics (e.g., Fig. 9d,e). There are no pulse-like motions detected among the 26 October 2016 M_w 5.9 shock recordings, which confirms the well-established observation that pulse occurrence is an uncertain event and thus a probabilistic function of source-to-site geometry (e.g., Iervolino and Cornell, 2008). The positions of the sites where evidence of pulse-like directivity is found, relative to the finite-fault geometry of the M_w 6.0 (Tinti *et al.*, 2016) and M_w 6.5 shocks (E. Tinti, personal comm., 2017), can be seen in Figure 9b,c. Most of the pulse-like features at these stations are generally oriented toward the fault-normal direction with small deviations that are not unheard-of for dip-slip events (the exception being T1201, wich exhibits a clear pulse mostly along the strike's orientation). Generally speaking, the results obtained in this study confirm the larger variability of the orientation of near-source pulses in dip-slip events when compared with the fault-normal pulse predominance in strike-slip faulting.

An important parameter that characterizes impulsive motions is the pulse duration (or pulse period, T_p), which is known to scale with earthquake magnitude (Somerville, 2003). This seems also confirmed by the pulse-like records detected within the central Italy sequence, as made evident from Fig-

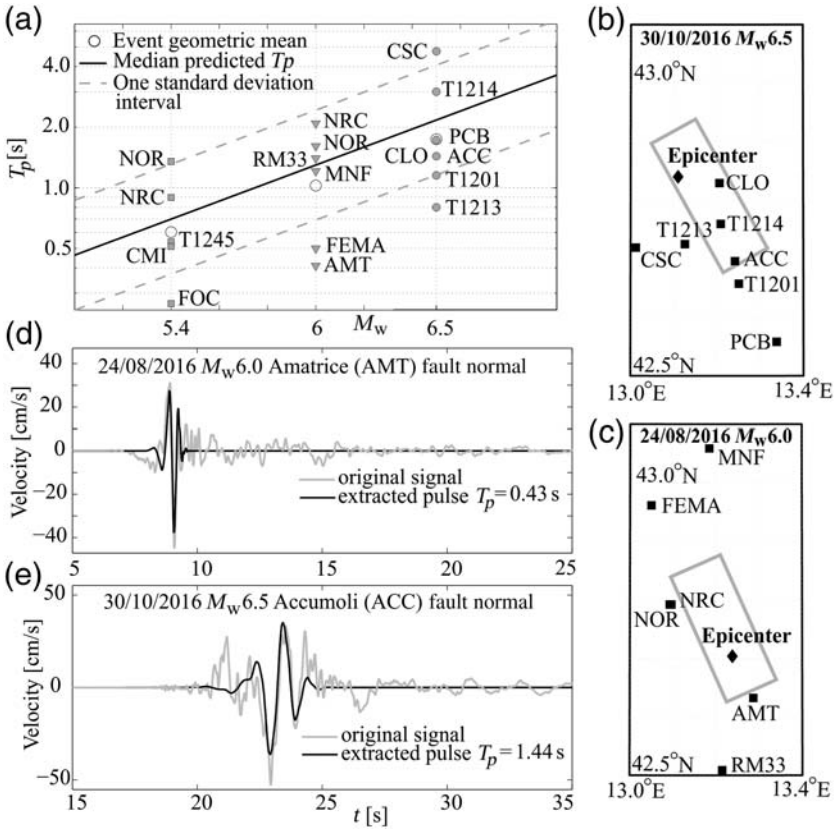

▲ **Figure 9.** (a) Pulse periods (T_p) for three events of the sequence plotted against magnitude compared with the predictive model by Baltzopoulos *et al.* (2016); (b) surface projection of fault plane and station locations where pulses likely related to directivity were detected for the M_w 6.5 Norcia shock; (c) the M_w 6.0 Amatrice shock; (d) velocity time series of the fault-normal component of ground motion with the extracted pulse for AMT station; and (e) ACC station.

ure 9a, in which the observed pulse durations fit with the empirical regression model versus magnitude calibrated by Baltzopoulos *et al.* (2016). It is also worth mentioning that existing empirical models for pulse-like directivity effects have been calibrated prevalently on data from events with strike-slip or reverse focal mechanisms; as such, data from normal faulting are a welcome addition to complete the picture.

Fling Step

Fling-step evaluations are important for engineering analysis, especially in cases of structures situated in the proximity of an extended fault. Standard strong-motion processing generally removes the fling effect in near-source records, due to the application of a high-pass filter. To recover the permanent displacement, different processing schemes based on baseline adjustments should be preferred. These schemes imply subtracting one or more baselines (straight lines or high-order polynomials) from the velocity trace before computing the displacement. We apply the piecewise baseline correction implemented in the BASeline COrrection (BASCO) code (Paolucci *et al.*, 2008; R. Paolucci, personal comm., 2015) to the strong-motion waveforms of the M_w 6.5 Norcia earthquake recorded by 19 stations with R_{JB} less than 15 km (Fig. 10a). The velocity traces are visually inspected to identify two time windows, one before and one after the strong-shaking phase, that are fitted by a first-order polynomial.

The larger permanent displacements (> 20 cm) are found in correspondence to the surface projection of the fault plane (Fig. 10a) on both the horizontal and vertical components (Fig. 9b). This result matches the Global Positioning System (GPS) observations (see Data and Resources) that revealed subsidence larger than 15 cm at stations over the fault projection.

The maximum permanent displacements are observed at station CLO (−80 cm on the vertical component and −60 cm on the east [E] component), in correspondence to the maximum slip patch identified by the source inversion study (E. Tinti, personal comm., 2017), which unfortunately cannot be compared with GPS observations. The permanent displacement inferred from strong-motion data is comparable with GPS measurement only when stations are close together (e.g., GPS station ARQT and accelerometric station T1214). In cases of stations far apart, only the direction of displacement can be compared (e.g., MMO and VETT and horizontal values for CSC and LNSS, as the permanent vertical displacements are negligible).

CONCLUSIONS

Since August 2016, central Italy has been struck by one of the most important seismic sequences ever recorded in the country. Until December 2016, three main events with magnitude larger than 5.9 occurred along the same fault zone. The strong-motion data set consisting of nearly 10,000 waveforms, available at the ESM database (see Data and Resources), allowed the analysis of the main features of the ground motion, in terms of distribution of shaking, ground-motion variability, and near-source ground-motion characterization.

The shake maps of the three events highlight an anisotropic spatial distribution of the ground motion. High-frequency ground-motion values decay fairly rapidly toward SW, whereas they appear to be less attenuated in the sector spanning from NW to NE. However, the areas of maximum shaking appear to reflect the complexities of the rupture on the finite faults. At low frequency, the ground motion amplifies in correspondence to the intramountain basins and the Plio–Pleistocene sedimentary deposits on the Adriatic coast.

The residual analysis reveals a ground-motion attenuation that is stronger than the regional trend by Bindi *et al.* (2011) at distances larger than 60 km. Large ground-motion variability is observed along the Apennine direction (NW–SE), which reflects the regional tectonic trend. This behavior can be attrib-

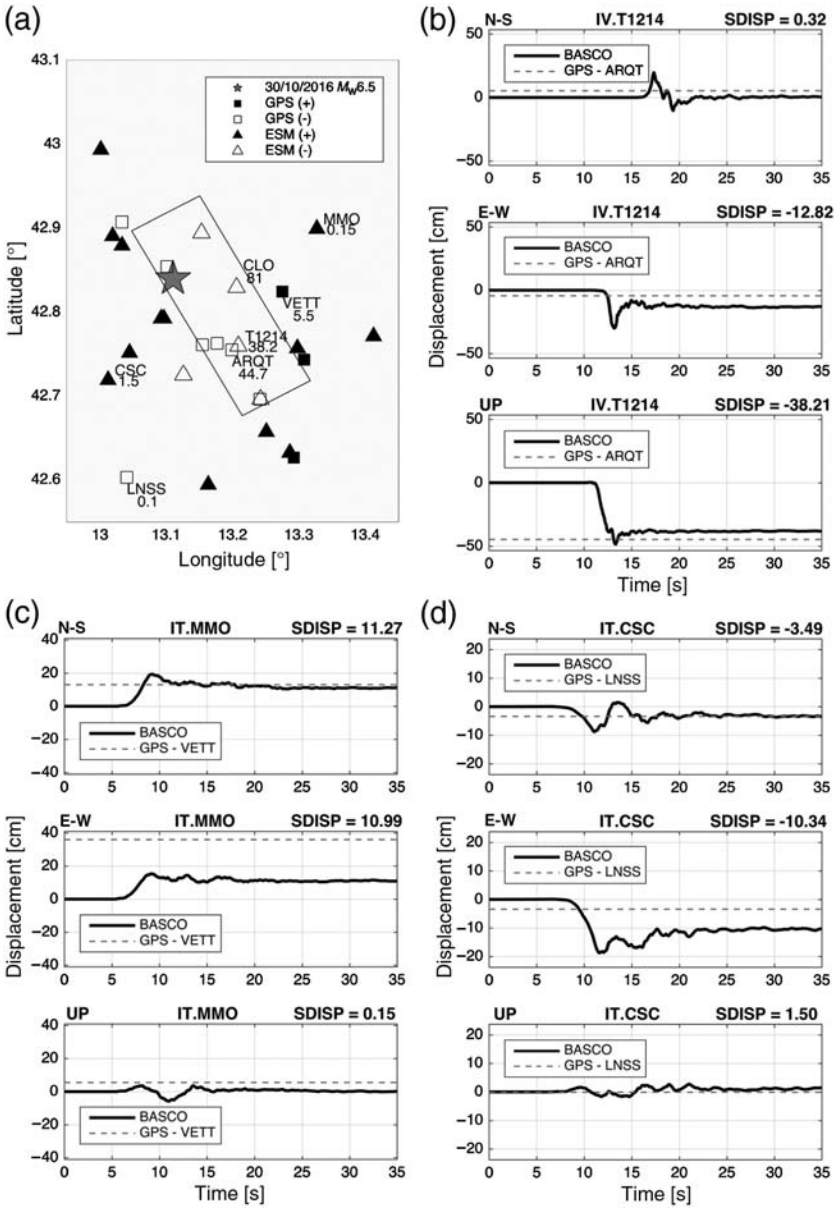

▲ **Figure 10.** Permanent displacement associated with the M_w 6.5 Norcia earthquake. (a) Surface projection of the fault and vertical permanent displacement from Global Positioning System (GPS, squares) and accelerometric stations (ESM, triangles); empty symbols are negative values (downward), whereas filled symbols are positive values (upward); (b–d) examples of displacement time series processed with the BASeline COrrection (BASCO) software (black lines), compared with the permanent displacement observed at the nearest GPS station (gray dotted lines); SDISP, permanent displacement (in centimeters). N-S, north–south; E-W, east–west.

uted to source-directivity effects, especially evident in the case of small-magnitude aftershocks that deserve a dedicated in-depth analysis.

The comparison with the design response spectra of the Italian seismic code shows that the spectra associated with the ground motions recorded in the epicentral area exceed the design actions in a range of short-to-medium vibration periods, as expected for this kind of earthquakes. On the other hand, also expected, the fraction of records above design intensities is relatively small and is mainly observed in the near fault.

Parsing near-source ground motions recorded during the strongest events in the sequence revealed evidence of possible pulse-like directivity effects in 18 ground velocity records. Pulse durations calculated for these waveforms fit well with previously proposed empirical models. The permanent displacements obtained from accelerometric records and GPS coseismic displacement are also comparable when the strong-motion waveforms are appropriately processed.

DATA AND RESOURCES

The locations of the seismic events of the central Italy sequence are obtained from Centro Nazionale Terremoti–Istituto Nazionale di Geofisica e Vulcanologia (CNT-INGV; http://cnt.rm.ingv.it, last accessed February 2017). Moment magnitude and focal mechanisms are obtained from the Time Domain Moment Tensor–Istituto Nazionale di Geofisica e Vulcanologia (TDMT-INGV; http://cnt.rm.ingv.it/tdmt, last accessed February 2017). The sources of the finite rupture models are Tinti *et al.* (2016) and Chiaraluce *et al.* (2017). The coseismic displacements are obtained from the INGV-Rete Integrata Nazionale Global Positioning System (GPS) (RING) network (http://ring.gm.ingv.it, last accessed February 2017). The unprocessed strong-motion data are obtained from the Rete Accelerometrica Nazionale (RAN), managed by the Department of Civil Protection (DPC; http://ran.protezionecivile.it/, last accessed February 2017) and from the INGV International Federation of Digital Seismograph Networks (FDSN) webservice (http://webservices.rm.ingv.it/, last accessed February 2017). The processed strong-motion data and station metadata are obtained from the Engineering Strong-Motion (ESM) database (http://esm.mi.ingv.it, last accessed February 2017). The flatfile with the strong-motion parameters is available at http://esm.mi.ingv.it/flatfile-2017/. The shake maps are available at http://shakemap.rm.ingv.it (last accessed February 2017). The 1:100,000 scale Italian geological map, compiled and published by the Servizio Geologico Nazionale, is available at http://www.apat.gov.it/Media/carta_geologica_italia/default.htm.

ACKNOWLEDGMENTS

The work presented in this article was developed in part within the activities of Rete dei Laboratori Universitari di Ingegneria

Sismica (ReLUIS) for the research program funded by the Dipartimento della Protezione Civile (2014–2018). Station metadata and shake map contribution are partly funded within the agreement between the Istituto Nazionale di Geofisica and Dipartimento della Protezione Civile for the seismic monitoring of Italy (Allegato A and B2, 2015–2016). The authors would like to acknowledge Editor-in-Chief Zhigang Peng, and Emel Seyhan, who both contributed toward improving the quality of this article.

REFERENCES

Abrahamson, N. A., and P. G. Somerville (1996). Effects of the hanging wall and footwall on ground motions recorded during the Northridge earthquake, *Bull. Seismol. Soc. Am.* **86,** S93–S99.

Abrahamson, N. A., W. J. Silva, and R. Kamai (2014). Summary of the ASK14 ground motion relation for active crustal regions, *Earthq. Spectra* **30,** no. 3, 1025–1055.

Akkar, S., and J. J. Bommer (2010). Empirical equations for the prediction of PGA, PGV, and spectral accelerations in Europe, the Mediterranean region, and the Middle East, *Seismol. Res. Lett.* **81,** no. 2, 195–206, doi: 10.1785/gssrl.81.2.195.

Akkar, S., M. A. Sandıkkaya, M. Şenyurt, A. Azari Sisi, B. Ö. Ay, P. Traversa, J. Douglas, F. Cotton, L. Luzi, B. Hernandez, *et al.* (2013). Reference database for seismic ground-motion in Europe (RESORCE), *Bull. Earthq. Eng.* **12,** no. 1, 311–339, doi: 10.1007/s10518-013-9506-8.

Al Atik, L., N. A. Abrahamson, J. J. Bommer, F. Scherbaum, F. Cotton, and N. Kuehn (2010). The variability of ground-motion prediction models and its components, *Seismol. Res. Lett.* **81,** no. 5, 794–801, doi: 10.1785/gssrl.81.5.794.

Baker, J. W. (2007). Quantitative classification of near-fault ground motions using wavelet analysis, *Bull. Seismol. Soc. Am.* **97,** no. 5, 1486–1501.

Baltzopoulos, G., D. Vamvatsikos, and I. Iervolino (2016). Analytical modelling of near-source pulse-like seismic demand for multi-linear backbone oscillators, *Earthq. Eng. Struct. Dynam.* **45,** no. 11, 1797–1815.

Bindi, D., M. Massa, L. Luzi, G. Ameri, F. Pacor, R. Puglia, and P. Augliera (2014). Pan-European ground-motion prediction equations for the average horizontal component of PGA, PGV, and 5%-damped PSA at spectral periods up to 3.0 s using the RESORCE dataset, *Bull. Earthq. Eng.* **12,** no. 1, 391–430, doi: 10.1007/s10518-013-9525-5.

Bindi, D., F. Pacor, L. Luzi, R. Puglia, M. Massa, G. Ameri, and R. Paolucci (2011). Ground motion prediction equations derived from the Italian strong motion database, *Bull. Earthq. Eng.* **9,** 1899–1920.

Bolt, B. A. (2006). Engineering seismology, in *Earthquake Engineering: From Engineering Seismology to Performance-Based Engineering*, Y. Bozorgnia and V. V. Bertero (Editors), CRC Press, Boca Raton, Florida.

Boore, D. M., and J. J. Bommer (2005). Processing of strong-motion accelerograms: Needs, options and consequences, *Soil Dynam. Earthq. Eng.* **25,** 93–115, doi: 10.1016/j.soildyn.2004.10.007.

Boncio, P., and G. Lavecchia (2000). A structural model for active extension in central Italy, *J. Geodyn.* **29,** 233–244.

Boncio, P., G. Lavecchia, and B. Pace (2004). Defining a model of 3D seismogenic sources for seismic hazard assessment applications: The case of central Apennines (Italy), *J. Seismol.* **8,** 407–425.

Borcherdt, T. (1994). Estimates of site-dependent response spectra for design (methodology and justification), *Earthq. Spectra* **10,** 617–653.

Calamita, F., and A. Pizzi (1994). Recent and active extensional tectonics in the southern Umbro-Marchean Apennines (central Italy), *Mem. Soc. Geol. Ital.* **48,** 541–548.

Cauzzi, C., E. Faccioli, M. Vanini, and A. Bianchini (2015). Updated predictive equations for broadband (0.01–10 s) horizontal response spectra and peak ground motions, based on a global dataset of digital acceleration records, *Bull. Earthq. Eng.* 1587–1612, doi: 10.1007/s10518-014-9685-y.

Cello, G., S. Mazzoli, E. Tondi, and E. Turco (1997). Active tectonics in the central Apennines and possible implications for seismic hazard analysis in peninsular Italy, *Tectonophysics* **272,** 43–68.

Chiaraluce, L., R. Di Stefano, E. Tinti, L. Scognamiglio, M. Michele, E. Casarotti, M. Cattaneo, P. De Gori, C. Chiarabba, G. Monachesi, *et al.* (2017). The 2016 central Italy seismic sequence: A first look at the mainshocks, aftershocks, and source models, *Seismol. Res. Lett.* **88,** no. 3, 757–771, doi: 10.1785/0220160221.

CS.LL.PP. (2008). Decreto Ministeriale 14 Gennaio 2008: Norme tecniche per le costruzioni, *Gazzetta Ufficiale della Repubblica Italiana* 29 (in Italian).

Darragh, R. B., J. P. Stewart, E. Seyhan, W. J. Silva, B. S. J. Chiou, K. E. Wooddell, R. W. Graves, A. R. Kottke, T. D. Ancheta, D. M. Boore, *et al.* (2014). NGA-West2 database, *Earthq. Spectra* **30,** no. 3, 989–1005.

Di Capua, G., G. Lanzo, V. Pessina, S. Peppoloni, and G. Scasserra (2011). The recording stations of the Italian strong motion network: Geological information and site classification, *Bull. Earthq. Eng.* **9,** no. 6, 1779–1796, doi: 10.1007/s10518-011-9326-7.

Donahue, J. L., and N. A. Abrahamson (2014). Simulation-based hanging wall effects, *Earthq. Spectra* **30,** no. 3, 1269–1284.

Dreger, D. S., and D. V. Helmberger (1993). Determination of source parameters at regional distances with three-component sparse network data, *J. Geophys. Res.* **98,** 8107–8125.

Eurocode 8 (2003). Design of structures for earthquake resistance– Part 1: General rules seismic actions and rules for buildings, EN 1998-1, European Committee for Standardization (CEN).

Faenza, L., and A. Michelini (2010). Regression analysis of MCS intensity and ground motion parameters in Italy and its application in ShakeMap, *Geophys. J. Int.* **180,** no. 3, 1138–1152, doi: 10.1111/j.1365-246X.2009.04467.x.

Felicetta, C., M. D'Amico, G. Lanzano, R. Puglia, E. Russo, and L. Luzi (2017). Site characterization of Italian accelerometric stations, *Bull. Earthq. Eng.* **15,** no. 6, 2329–2348, doi: 10.1007/s10518-016-9942-3.

Galadini, F., and P. Galli (2000). Active tectonics in the central Apennines (Italy)—Input data for seismic hazard assessment, *Nat. Hazards* **22,** 225–270.

Huang, M. H., E. J. Fielding, C. Liang, P. Milillo, D. Bekaert, D. Dreger, and J. Salzer (2017). Coseismic deformation and triggered landslides of the 2016 M_w 6.2 Amatrice earthquake in Italy, *Geophys. Res. Lett.*, **44,** no. 3, 1266–1274, doi: 10.1002/2016GL071687.

Iervolino, I. (2013). Probabilities and fallacies: Why hazard maps cannot be validated by individual earthquakes, *Earthq. Spectra* **29,** no. 3, 1125–1136.

Iervolino, I., and C. A. Cornell (2008). Probability of occurrence of velocity pulses in near-source ground motions, *Bull. Seismol. Soc. Am.* **98,** no. 5, 2262–2277.

Iervolino, I., G. Baltzopoulos, and E. Chioccarelli (2016). Preliminary engineering analysis of the August 24th 2016, ML 6.0 Central Italy earthquake records, *Ann. Geophys.* **59,** Fast Track 5, doi: 10.4401/ag-7182.

Iervolino, I., E. Chioccarelli, and G. Baltzopoulos (2012). Inelastic displacement ratio of near-source pulse-like ground motions, *Earthq. Eng. Struct. Dynam.* **41,** 2351–2357.

Istituto Nazionale di Geofisica e Vulcanologia (INGV) Seismological Data Centre (1997). Rete Sismica Nazionale (RSN), Istituto Nazionale di Geofisica e Vulcanologia (INGV), Italy, doi: 10.13127/SD/X0FXnH7QfY.

Joyner, W. B., and D. M. Boore (1981). Peak horizontal acceleration and velocity from strong motion records including records from the 1979 Imperial Valley, California, earthquake, *Bull. Seismol. Soc. Am.* **71,** no. 6, 2011–2038.

Kaklamanos, J., L. G. Baise, and D. M. Boore (2011). Estimating unknown input parameters when implementing the NGA ground-

motion prediction equations in engineering practice, *Earthq. Spectra* **27,** no. 4, 1219–1235, doi: 10.1193/1.3650372.

Lavecchia, G., P. Boncio, F. Brozzetti, M. Stucchi, and I. Leschiutta (2002). New criteria for seismotectonic zoning in central Italy: Insights from the Umbria-Marche Apennines, *Boll. Soc. Geol. Ital.* **1,** 881–890.

Lavecchia, G., F. Brozzetti, M. Barchi, M. Menichetti, and J. V. A. Keller (1994). Seismotectonic zoning in east-central Italy deduced from an analysis of the Neogene to present deformations and related stress fields, *Geol. Soc. Am. Bull.* **106,** 1107–1120.

Luzi, L., D. Bindi, R. Puglia, F. Pacor, and A. Oth (2014). Single-station sigma for Italian strong-motion stations, *Bull. Seismol. Soc. Am.* **104,** 467–483.

Michelini, A., L. Faenza, V. Lauciani, and L. Malagnini (2008). ShakeMap implementation in Italy, *Seismol. Res. Lett.* **79,** no. 5, 688–697, doi: 10.1785/gssrl.79.5.688.

Paolucci, R., F. Pacor, R. Puglia, G. Ameri, C. Cauzzi, and M. Massa (2011). Record processing in ITACA, the new Italian strong motion database, in *Earthquake Data in Engineering Seismology*, in Geotechnical, Geological and Earthquake Engineering Series, S. Akkar, P. Gulkan, and T. Van Eck (Editors), Vol. 14, Springer, Dordrecht, The Netherlands, 99–113.

Paolucci, R., A. Rovelli, E. Faccioli, C. Cauzzi, D. Finazzi, M. Vanini, C. Di Alessandro, and G. Calderoni (2008). On the reliability of long-period response spectral ordinates from digital accelerograms, *Earthq. Eng. Struct. Dynam.* **37,** 697–710, doi: 10.1002/eqe.781.

Presidency of the Council of Ministers, Civil Protection Department (1972). Italian strong motion network, Presidency of Council of Ministers–Civil Protection Department, Other/Seismic Network, doi: 10.7914/SN/IT.

Pucci, S., P. M. De Martini, R. Civico, F. Villani, R. Nappi, T. Ricci, R. Azzaro, C. A. Brunori, M. Caciagli, F. R. Cinti, *et al.* (2017). Coseismic ruptures of the 24 August 2016, M_w 6.0 Amatrice earthquake (central Italy), *Geophys. Res. Lett.* **44,** 2138–2147, doi: 10.1002/2016GL071859.

ReLUIS-Istituto Nazionale di Geofisica e Vulcanologia (INGV) Working Group (2016). Preliminary study of Rieti earthquake ground motion records V6, available at http://www.reluis.it (last accessed July 2017).

Rodriguez-Marek, A., G. A. Montalva, F. Cotton, and F. Bonilla (2011). Analysis of single-station standard deviation using the KiK-net data, *Bull. Seismol. Soc. Am.* **101,** 1242–1258.

Scognamiglio, L., E. Tinti, A. Michelini, D. S. Dreger, A. Cirella, M. Cocco, S. Mazza, and A. Piatanesi (2010). Fast determination of moment tensors and rupture history: What has been learned from the 6 April 2009 L'Aquila earthquake sequence, *Seismol. Res. Lett.* **81,** no. 6, 892–906, doi: 10.1785/gssrl.81.6.892.

Scognamiglio, L., E. Tinti, and M. Quintiliani (2016). The first month of the 2016 central Italy seismic sequence: Fast determination of time domain moment tensors and finite fault model analysis of the M_L 5.4 aftershock, *Ann. Geophys.* **59,** Fast Track 5, doi: 10.4401/ag-7246.

Somerville, P. G. (2003). Magnitude scaling of the near fault rupture directivity pulse, *Phys. Earth Planet. In.* **137,** 201–212.

Somerville, P. G., N. F. Smith, R. W. Graves, and N. A. Abrahamson (1997). Modification of empirical strong ground motion attenuation relations to include the amplitude and duration effects of rupture directivity, *Seismol. Res. Lett.* **68,** 199–222.

Spudich, P., B. Rowshandel, S. K. Shahi, J. W. Baker, and B. S. J. Chiou (2014). Comparison of NGA-West2 directivity models, *Earthq. Spectra* **30,** no. 3, 1199–1221.

Stucchi, M., C. Meletti, V. Montaldo, H. Crowley, G. M. Calvi, and E. Boschi (2011). Seismic hazard assessment (2003–2009) for the Italian building code, *Bull. Seismol. Soc. Am.* **101,** 1885–1911.

Tinti, E., L. Scognamiglio, A. Michelini, and M. Cocco (2016). Slip heterogeneity and directivity of the M_L 6.0, 2016, Amatrice earthquake estimated with rapid finite-fault inversion, *Geophys. Res. Lett.* **43,** no. 20, 10,745–10,752, doi: 10.1002/2016GL071263.

Vezzani, L., A. Festa, and F. C. Ghisetti (2010). Geology and tectonic evolution of the central-southern Apennines, Italy, *Geol. Soc. Am. Spec. Pap.* **469,** 58 pp., accompanying CD-ROM with geological maps at scale 1:250,000.

Wald, D. J., V. Quitoriano, T. H. Heaton, H. Kanamori, C. W. Scrivner, and C. B. Worden (1999). TriNet ShakeMaps: Rapid generation of peak ground motion and intensity maps for earthquakes in southern California, *Earthq. Spectra* **15,** no. 3, 537–555, doi: 10.1193/1.1586057.

Wells, D. L., and K. J. Coppersmith (1994). New empirical relationships among magnitude, rupture length, rupture width, rupture area, and surface displacement, *Bull. Seismol. Soc. Am.* **84,** no. 4, 974–1002.

Lucia Luzi
Francesca Pacor
Rodolfo Puglia
Giovanni Lanzano
Chiara Felicetta
Maria D'Amico
Istituto Nazionale di Geofisica e Vulcanologia (INGV)
via Corti 12
20133 Milan, Italy
lucia.luzi@ingv.it
francesca.pacor@ingv.it
rodolfo.puglia@ingv.it
giovanni.lanzano@ingv.it
chiara.felicetta@ingv.it
maria.damico@ingv.it

Alberto Michelini
Licia Faenza
Valentino Lauciani
Istituto Nazionale di Geofisica e Vulcanologia (INGV)
via di Vigna Murata 605
00143 Rome, Italy
alberto.michelini@ingv.it
licia.faenza@ingv.it
valentino.lauciani@ingv.it

Iunio Iervolino
Dipartimento di Strutture per l'Ingegneria e l'Architettura
Università degli Studi di Napoli Federico II
Via Claudio 21
80125 Naples, Italy
iunio.iervolino@unina.it

George Baltzopoulos
Eugenio Chioccarelli
Istituto per le Tecnologie della Costruzione–Consiglio Nazionale delle Ricerche (ITC-CNR)
URT at Dipartimento di Strutture per l'Ingegneria e l'Architettura
Università degli Studi di Napoli Federico II
Via Claudio 21
80125 Naples, Italy
baltzopoulos@itc.cnr.it
chioccarelli@itc.cnr.it

Published Online 9 August 2017